N-TiO$_2$ Photocatalysts highly active under visible irradiation for NO$_X$ abatement and 2-propanol oxidation

R. Amadelli[a,*], L. Samiolo[a], M. Borsa[b], M. Bellardita[c,d], L. Palmisano[c,d,*]

[a] CNR-ISOF, U.O.S. of Ferrara, c/o Department of Chemistry, University of Ferrara, via L. Borsari, 46–44121 Ferrara, Italy
[b] CTG-Italcementi, Via Camozzi, 124, 24121 Bergamo, Italy
[c] "Schiavello-Grillone" Photocatalysis Group, Dipartimento di Ingegneria Elettrica, Elettronica e delle Telecomunicazioni di tecnologie Chimiche, Automatica e modelli Matematici (DIEETCAM), University of Palermo, Viale delle Scienze, 90128 Palermo, Italy
[d] Consorzio Interuniversitario La Chimica per l'Ambiente, Via delle Industrie 21/8, 30175 Marghera, Italy

ABSTRACT

N-doped TiO$_2$ powders were prepared by two different sol–gel methods. Samples were characterised by X-ray diffraction (XRD), BET specific surface area measurements (SSA), scanning electron microscopy (SEM), diffuse reflectance spectroscopy (DRS), X-ray photoelectron spectroscopy (XPS) and Electron Paramagnetic Resonance (EPR). XPS measurements revealed a signal at 400 eV assignable to nitrogen in the form of Ti—N—O. EPR signals are attributed to molecular NO trapped with cavities/defects possibly interacting with oxygen vacancies. The photocatalytic activity under UV and visible light was determined following the abatement of NO$_x$ and the photodegradation of 2-propanol in gas–solid systems. N-doped TiO$_2$ showed a higher activity compared with the pristine commercial and home prepared samples under visible light irradiation. A good photoactivity in the abatement of both NO$_x$ and 2-propanol is also observed for mechanical dispersions of N-TiO$_2$ in CaCO$_3$ serving as a model in view of perspective application in photocatalytically active construction and architectural materials.

© 2012 Elsevier B.V. All rights reserved.

1. Introduction

It is now recognised that anion doping is a promising strategy to improve the visible light photoactivity of TiO$_2$, itself absorbing only a small fraction of solar radiation. In this context, the case of nitrogen doping, in particular, is attracting considerable attention. It is possible to cite but representative works [1–6] because of the volcanic research activity in this field, especially following the publication by Asahi et al. [7], although a paper by Hirai et al. that appeared as early as 1978 merits to be cited [8].

Reasons for the observed visible light activity of nitrogen-doped TiO$_2$ (N-TiO$_2$) are a matter of considerable debate [4,9–13] although an explanation based on the simultaneous presence of substitutional or interstitial nitrogen and oxygen vacancies (V$_O^\bullet$) is gaining popularity lately [14–16].

Comparison of experimental results is hampered by several facts, among which: (i) the preparation methods are diverse and consequently the properties of the resulting materials vary considerably, which makes it difficult to compare results; (ii) the methods to test for visible light activity vary, with no standard test being employed [17].

Contrasting data on the visible light photocatalytic activity of these materials is even more conspicuous but it seems possible to state that their catalytic activity at the gas–solid interphase under visible light illumination is good. Comprehensive surveys on air purification by photocatalysis have been published recently [18–22].

For the specific case of N-TiO$_2$ research is focussed on the photodegradation of different gaseous pollutants such as NO$_x$ [15,23–25] and VOCs including acetone [26], propylene [14], thichloroethylene [27], benzene/toluene [28] and 2-propanol [29,30]. Results are stimulating but it is, however, difficult to draw general conclusions because of the drawbacks cited above, in particular the fact that, typically, the photooxidation of one type model pollutant is generally examined.

In the present work, we report on the visible light photocatalytic behaviour of N-TiO$_2$ toward the abatement of gaseous pollutants. Specifically, we examine the photocatalytic conversion of NO$_x$ (NO + NO$_2$) since it is an ubiquitous air pollutant, and the photodegradation of 2-propanol as a model VOC species. For the sake of a systematic approach, we adopted the sol–gel method for preparation of N-TiO$_2$ as in our previous works [16,31], mainly using TiOSO$_4$. Herein we also examine the behaviour of N-TiO$_2$ in CaCO$_3$ matrices in view of perspective application in photoactive

* Corresponding authors at: Dipartimento di Ingegneria Elettrica, Elettronica e delle Telecomunicazioni di tecnologie Chimiche, Automatica e modelli Matematici (DIEETCAM), University of Palermo, Viale delle Scienze, 90128 Palermo, Italy; CNR-ISOF, U.O.S. of Ferrara, c/o Department of Chemistry, University of Ferrara, via L. Borsari, 46–44121 Ferrara, Italy.
E-mail addresses: amr@unife.it (R. Amadelli), leonardo.palmisano@unipa.it (L. Palmisano).

Table 1
Sol–gel preparation of TiO_2 and $N-TiO_2$ from $TiOSO_4$ by hydroxide addition.

Sample	End pH	mol N/mol Ti	Hydroxide
S0	7	0	NaOH
S1	5.5	6.4	NH_4OH
S2	7	6.7	NH_4OH
S3	9	8.5	NH_4OH
SU[a]		8.0	

[a] Prepared by hydrolysis of an ethanol solution of Ti iso-propoxide and urea.

construction materials. With this purpose in mind, we compare the $N-TiO_2$ with some commercial anatase samples that are commonly employed to obtain materials (e.g. concrete) with de-pollution properties.

2. Experimental

2.1. Photocatalysts preparation

The precursor is a $TiOSO_4$ solution (5% Ti w/w in 27–30% H_2SO_4, Fluka). In a typical preparation, 16 mL of the precursor solution are added to 800 mL of triply distilled water under vigorous stirring. The measured pH of this solution was 1.2–1.3. Ammonium hydroxide (25%, Fluka) or NaOH in one case, is then added drop wise to the $TiOSO_4$ acid solution until a desired pH (Table 1) is reached. In all preparations, the resulting suspension is mechanically stirred at room temperature for 5 h and after at least 12 h decantation the liquid is removed. The precipitate is subsequently washed twice under stirring with 800 mL of a 0.23 M solution of NH_4OH and then dried in an oven at 100 °C.

Experiments have demonstrated that washing with the ammonia solution produces materials with better reproducible photocatalytic activity. It is important to fix the initial pH since this will determine the amount of added NH_4OH that is necessary to reach the final desired pH of the gel. For the case of sample S0 (Table 1), the gel was washed with triple distilled water only. All dried samples were finally calcined at 450 °C for 2 h yielding yellow powders for samples S1, S2 and S3.

For a comparative purpose, sample SU (Table 1) was prepared following a different sol–gel method involving hydrolysis of titanium iso-propoxide/urea solution in ethanol with the final calcination step as for the other samples.

2.2. Main equipment

XRD patterns of the powders were recorded at room temperature on a Bruker Instrument model D8, using the Cu Kα radiation and a graphite monochromator. X-ray diffraction was used for crystal phase identification and to evaluate the particle sizes. The crystallite size was estimated from the Scherrer formula: $\Phi = K\lambda/(\beta\cos\theta)$ where Φ is the crystallite size, λ is the wavelength of the X-ray radiation (0.154 nm), K is a constant usually taken as 0.89, β is the peak width at half-maximum height after subtraction of the equipment broadening.

The specific surface areas (SSA) of the powders were determined in a Flow Sorb 2300 apparatus (Micromeritics) by using the single-point BET method. The samples were degassed for 0.5 h at 250 °C prior to the measurement. SEM observations were obtained using a model Philips XL30 ESEM microscope, operating at 25 kV on specimens upon which a thin layer of gold had been evaporated.

Diffuse reflectance UV–vis spectra (DRS) were recorded at room temperature on a JASCO V-570 spectrophotometer equipped with an integrating sphere and $BaSO_4$ was used as reference. XPS data were recorded on a VG Escalab MkII instrument. EPR spectra

were registered at 90 K using a Bruker 220 SE spectrometer, at a microwave frequency of 9.4 GHz.

2.3. Methods

2.3.1. NO_x photo-oxidation

The experiments of photooxidation of nitrogen oxides were carried on 0.2 g of the powders spread onto Nylon disc supports (0.64 cm^2) located in a 3 L Pyrex glass reactor. This is connected to a 20 L mixing chamber and was irradiated with UV or visible light from a commercial lamp (Osram Vitalux 300 W) while a flux of air added with NO or a mixture of NO and NO_2 was continuously re-circulated (batch mode) [32] at a flow rate of 5 L min^{-1}. A set of cut-off filters was used to select the wavelength range while IR radiation was avoided by a water filter.

Concentrations of nitrogen oxides were measured at regular time intervals by the chemiluminescence method (Nitrogen Oxides Analyzer – Model 8440, Monitor Labs).

Some experiments on NO_x photo-oxidation have been carried out with commercial anatase TiO_2 (Millenium Chemicals).

2.3.2. Photo-oxidation of 2-propanol

The photoactivity of the samples was tested by evaluating the rate of degradation of 2-propanol in a Pyrex batch reactor ($\varnothing = 12.5$ cm; $V = 0.9$ dm^3) in gas–solid regimen under ultraviolet or visible light irradiation. Thin layers of the powders were prepared by spreading the slurries, obtained by mixing the powders with water, on glass supports that were subsequently dried at 323 K for 30 min.

For the runs carried out under UV light irradiation the powders were irradiated from the top by a 500 W medium pressure Hg lamp. A water filter was interposed between the lamp and the photoreactor to cut the infrared radiation. The light intensity at the film surface was 1.3 mW cm^{-2}.

The runs under visible light irradiation were carried out using a 1500 W Xenon lamp. Light of wavelength >400 nm was cut-off by a chemical filter (1 mol L^{-1} KNO_2 solution). In these experiments the light intensity at the film surface was 56 mW cm^{-2}. The reactor was saturated with O_2 and successively established amounts of 2-propanol were introduced into the vessel. Samples of 500 μL were withdrawn at fixed intervals using a gas tight syringe. 2-Propanol and acetone concentrations were determined by means of a GC Shimadzu 17 A equipped with a HP-1 column and a FID detector, using He as the carrier gas. The amount of CO_2 developed during the photodegradation was followed by using a GC HP 6890 equipped with a Supelco Carboxen^{TM} column.

3. Results and discussion

3.1. Structural characterisation

Fig. 1 shows a representative result of X-ray diffraction measurements on samples S0 to S3. Not unexpectedly, negligible morphological differences are observed by reason of the fact that the preparation conditions are the same except for the amount of NH_4OH used for the gel precipitation. All these samples are crystalline and constituted by 100% anatase. The samples area was 80 ± 5 m^2 g^{-1} and the average particle dimension 26.5 nm, as calculated from the mentioned Scherrer equation. The comparison sample SU was characterised by an area of 60 ± 5 m^2 g^{-1} and particle size of 30 nm. SEM images (Fig. 2) feature similar morphology and particles size distribution. Some aggregates of small particles of irregular shape is also observed.

Fig. 3 shows the diffuse reflectance spectra of the samples. The spectra for the samples containing nitrogen reveal higher absorption between 390 and 530 nm with respect to the pristine oxide
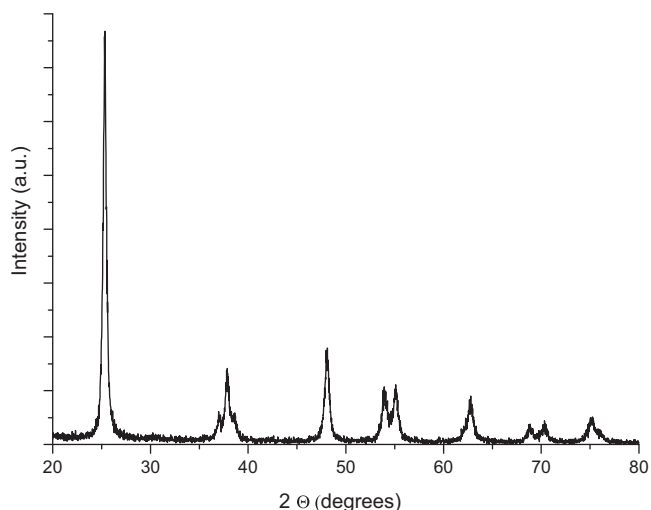
Fig. 1. Representative XRD pattern of N-TiO$_2$ prepared by hydrolysis of TiOSO$_4$ with NH$_4$OH and calcined at 450 °C for 2 h (samples S0 to S3).
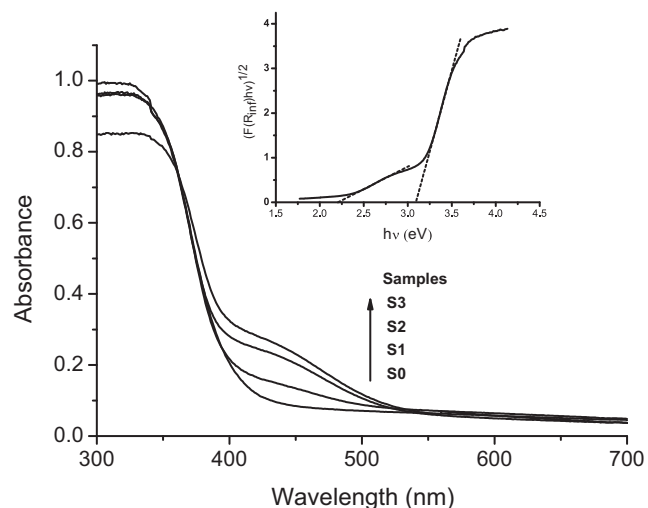

Fig. 3. Diffuse reflectance UV–visible spectra (DRS) of undoped and nitrogen-doped TiO$_2$ starting from different NH$_4^+$/Ti mol ratios. All samples calcined at 450 °C for 2 h. Inset: transformed K–M function ($[F(R_\infty)h\nu]^{1/2}$) versus the energy of the light absorbed.
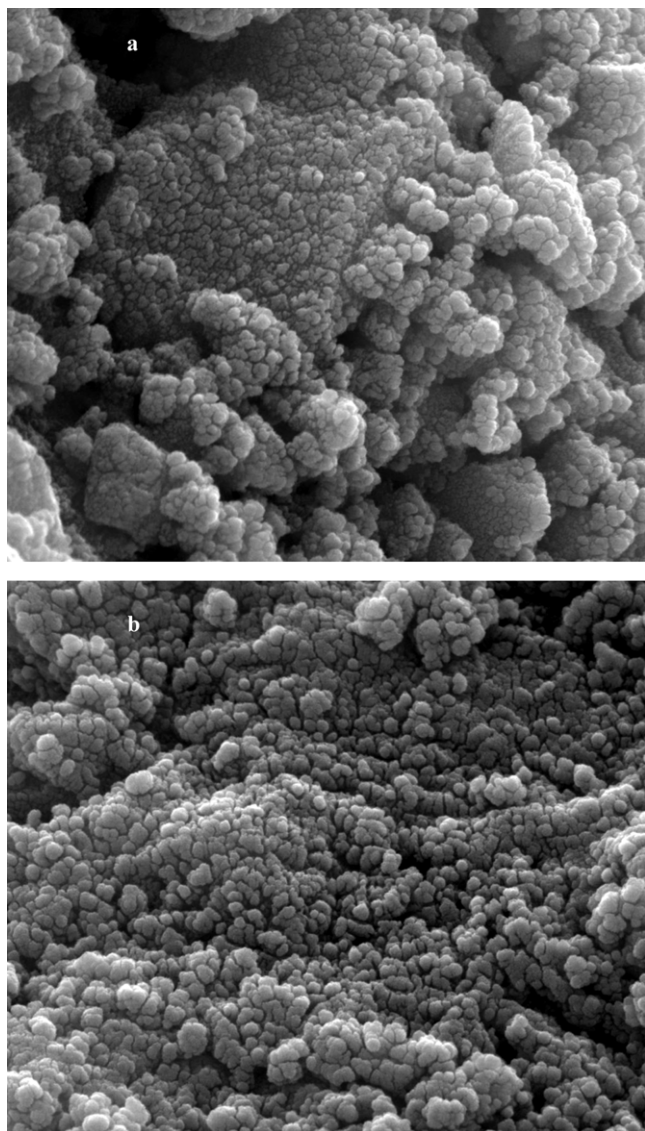
S0. Specifically, two absorption edges are observed in the plot of transformed K–M function ($[F(R_\infty)h\nu]^{1/2}$) (Fig. 3, inset), at 400 nm (3.1 eV) and 560 nm (2.21 eV). The first edge is related to the band structure of TiO$_2$ while the second one is probably associated to the presence of an energy band located above the valence band that induces the visible light activity. Then the presence of nitrogen does not appear to modify the band-gap value.

A representative XPS spectrum is displayed in Fig. 4 for sample S2. All other N-TiO$_2$ samples, including SU, reveal the same N 1s signal at ca. 400 eV which is commonly observed for nitrogen-doped TiO$_2$ prepared by the so-called wet methods [33], and is seemingly characteristic of nitrogen hosted in an interstitial position, directly bound to lattice oxygen (Ti—O—N) [4,34]. We could not analyse with the same confidence the different signals in terms of intensities on account of instrumental limitations. On the other hand, XPS analysis of N-TiO$_2$ materials often reveals very weak N 1s signals [26,35]
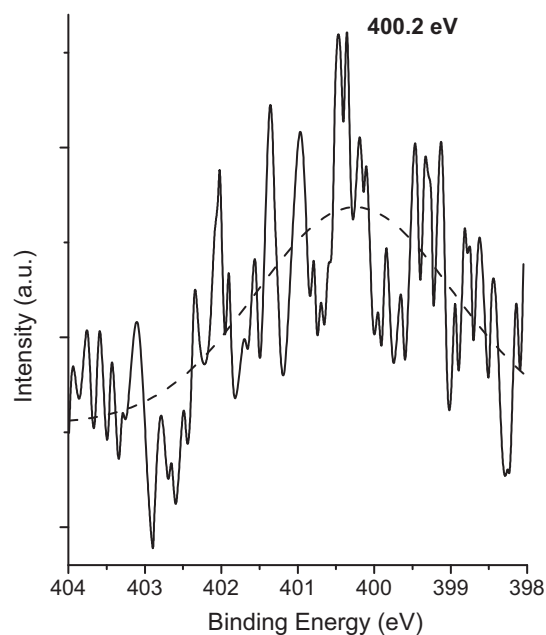

Fig. 2. SEM images of the samples S0 (a) and S2 (b). Magnification 100,000×.

Fig. 4. XPS spectra in the N1 s region for sol–gel prepared N-TiO$_2$ from TiOSO$_4$ and NH$_4$OH (sample S2, see text).
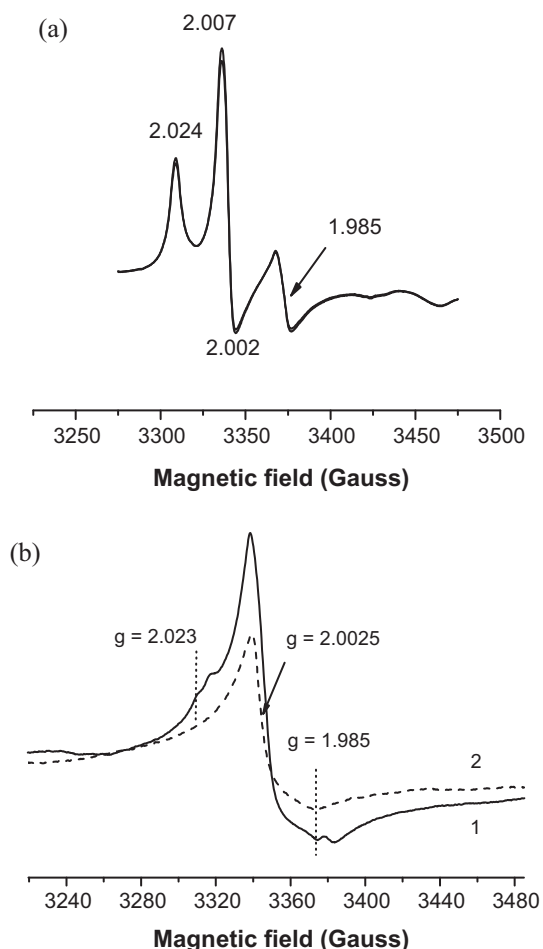
Fig. 5. EPR spectra of different TiO$_2$ samples at 90 K: (a) N-TiO$_2$ (sample SU); (b) spectrum 1 is N-TiO$_2$ (sample S2) obtained after calcinations at 450 °C for 2 h and spectrum 2 is obtained by annealing either N-TiO$_2$ (sample S2) or sample S0 (undoped TiO$_2$) at 600 °C for 1 h. See text for explanations.

and, in this context, it is to be noted that Orlov et al. [36] performed an angle resolved XPS analysis of N implanted TiO$_2$ and reported an effect of grazing angle on the signal detection, which is difficult to verify experimentally in the case of powders.

In Fig. 5 (a and b) are displayed typical low temperature EPR spectra of the same samples SU and S2 used in the XPS study. Illumination at λ > 400 nm did not result in appreciable changes in the spectra. On the basis of literature data [37,38], assignment of the EPR spectrum of sample SU reported in Fig. 5a is straightforward. It corresponds to molecular NO trapped within cavities/defects [37]. It is interesting to note that the same EPR signal is reported by Mei et al. [38], but only in the case of nitrogen-doped mesostructured TiO$_2$ where the radicals are stabilised at the surface of voids or pores.

The spectrum of sample S2 (Fig. 5b) is somewhat more complex but in part may also be ascribed to the presence of NO experiencing a higher dipolar interaction caused by a higher confinement degree within the mentioned cavities/defects. This can possibly explain the fact that the spectrum is clearly less resolved than that shown in Fig. 5a for sample SU. Actually, even a qualitative analysis of the spectrum (1) in Fig. 5b indicates that it is the result of different contributions, and oxygen vacancies (V$_0^\bullet$) represent a possible candidate. The spectrum has peaks at g = 2.023 and g = 1.985 which have been attributed to an interaction of V$_0^\bullet$ with NO [34,39]. In this context, we observed that annealing of both S2 or S0 at 600 °C yields white powders which show no N 1s XPS signal but give the same

low temperature EPR signal (spectrum 2 in Fig. 5b) with g = 2.0028, generally attributed to an electron trapped on an oxygen vacancy [39]. These annealed samples feature a high visible light response, yet the initially photoactivity is totally lost in subsequent runs with the same photocatalyst. This is indicative of an instability of V$_0^\bullet$ centres in the absence of the stabilising effect of nitrogen species. It has been, in fact, proposed that V$_0^\bullet$–NO–Ti are responsible for a high, stable photocatalytic activity in the visible [39,40].

3.2. Photocatalytic activity

3.2.1. Nitrogen oxides abatement

The photocatalytic oxidation of NO$_x$ involves reactions of the nitrogen oxides with surface active oxygen species [32,41] leading to formation of NO$_2$ from NO and conversion of NO$_2$ to adsorbed nitrate. These processes require interaction of reactants and intermediates with the surface. Adsorption phenomena involving NO are, by comparison with NO$_2$, less dominating and this explains why in several research works, aiming to assess materials photoactivity in nitrogen oxides removal, focus on NO as a substrate is preferred. Moreover, according to different reports, NO is predominant in the NO$_x$ close to emission sources (e.g., tunnel exhaust).

Fig. 6a shows that for 1 h experiments, using sample S2, NO conversion amounts to about 98% and 87% for irradiation at λ > 360 nm and λ > 450 nm, respectively. It is moreover interesting to add that

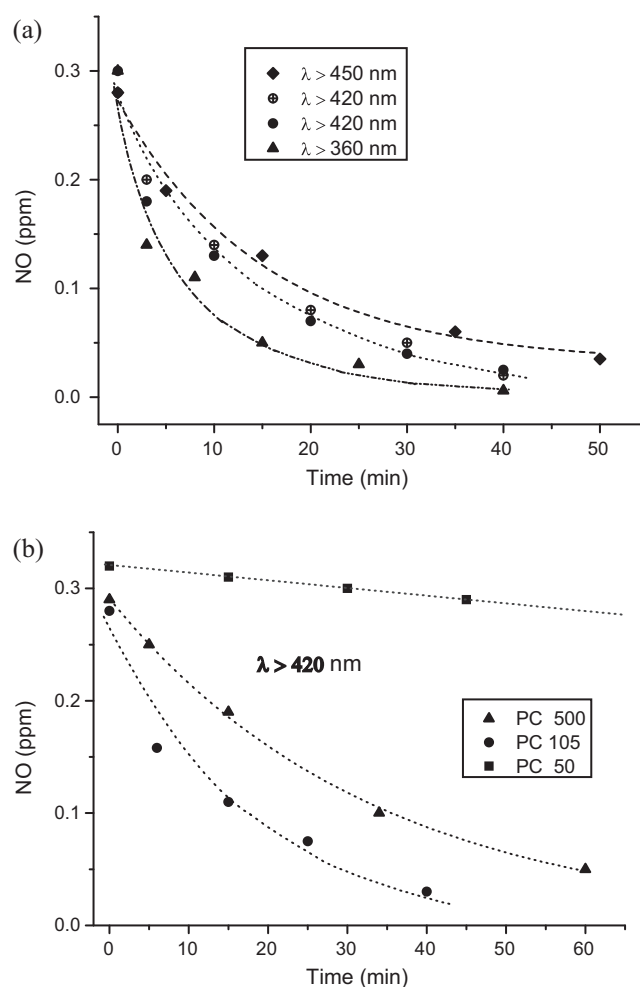**Fig. 6.** Removal of NO as a function of time under batch conditions: (a) on N-TiO$_2$ (sample S2; two measurements are shown for λ > 420 nm); (b) on commercial anatase TiO$_2$ (Millenium Chemicals). Irradiations in different wavelength regions selected with cut-off filters. Fixed incident light intensity $I° = 1.6 \pm 0.1$ mW cm^{-2}.

Table 2
Photonic yields for UV and visible light NO photooxidation on N-TiO$_2$ (sample S2).

Wavelength (nm)	Light intensity (Einstein s^{-1})[a]	Initial NO conversion rate (mol s^{-1})	Photonic efficiency (Φ)
365	4.69×10^{-11}	4.45×10^{-11}	0.95
436	1.45×10^{-11}	8.60×10^{-12}	0.59

[a] Corrected by the % absorption [$(R_0-R/R_0) \times 100$] from diffuse reflectance spectra.

the results observed for UV irradiation with sample S0 (not shown) are the same as those with S2. We can then conclude that there is no loss of photoactivity in the UV on N-TiO$_2$. In analogous experiments with samples S1 and S3 conversion at $\lambda > 450$ nm was 58% and 72%, respectively. It is noteworthy that sample S3 presents a lower photoactivity than the sample S2 despite the fact that it absorbs more visible light (Fig. 3) and this confirms the doubts of some authors on the extrapolation of photocatalytic activity from absorption spectra [42]. The photoactivity of sample SU from urea was also comparatively low and the forthcoming discussion will focus mainly on the results obtained with sample S2 which features the highest photoactivity.

Table 2 reports the photonic yields at fixed wavelengths in the UV ($\lambda = 365$ nm) and in the visible region ($\lambda = 436$ nm), calculated using the procedure described before [16]. The yields are based on initial rates of NO photoconversion on sample S2 and are rather high in the UV and in the visible too.

Fig. 6b shows results of NO conversion upon visible light irradiation ($\lambda > 420$ nm) of commercial TiO$_2$ samples (Millenium). In a comparative analysis of data, we noticed that PC 105 has a response to visible light and, unexpectedly, its photoactivity at $\lambda > 420$ nm was the same as that of N-TiO$_2$ (S2). Some visible activity is also noted for PC 500, and this interesting result cannot be imputed to the presence of rutile (all commercial samples consist of 100% anatase), nor can it be ascribed to surface area and particle size differences [43]. On the other hand, for irradiation at $\lambda > 450$ nm, PC 105 and PC 500 become inactive while the photocatalytic activity of N-TiO$_2$ is quite good (cf. Fig. 6a). The sub-bandgap response of some commercial anatase TiO$_2$ samples is an intriguing phenomenon which needs to be examined in more detail before explanations can be confidently formulated. However, one could speculate that the influence of vacancies (defects) on the observed photocatalytic behaviour would not represent a far-fetched explanation as, indeed, quite a few publications appeared reporting on enhanced photocatalytic NO$_x$ abatement on TiO$_2$ specially treated or prepared to increase the $V_0^\bullet$ concentration [25,44]. For the case of nitrogen-doped TiO$_2$ materials too, the formation of $V_0^\bullet$ and their contribution to visible light photoactivity is a recurring question [15,16,25]. Ihara et al. [26], in particular, compare the photocatalytic behaviour of N-TiO$_2$ with that of plasma treated TiO$_2$ and conclude that vacancies play a dominant role. They state that the role of nitrogen is that of stabilising oxygen-deficient sites, as also proposed in the more recent work [14,34,39,45].

We are currently carrying out photoluminescence measurements as they offer a powerful tool to investigate on intra bandgap energy states [46,47]. Preliminary results showed that sub-bandgap irradiation causes a clear emission in the visible at 500–600 nm with intensity in the order N-TiO$_2$ > PC 105 > PC 500. This green emission has been attributed to $V_0^\bullet$ [16,46,47] and in particular to F$^+$ centres [47], which would also be in keeping with mechanisms of NO$_x$ photo-oxidation processes involving vacancies [15,26].

The question has often been raised on whether the focus of photocatalytic tests on NO$_x$ abatement should be NO$_2$, NO or both. The former is, among nitrogen oxides, the one having the highest toxicological impact and it stands to reason that authorities having the task of enforcing limitations on NO$_x$ in the environment often refer to NO$_2$ as the target species. The use of NO/NO$_2$ mixtures sometimes provides valuable information as described in an interesting and informative paper by Sano et al. [23].

In photocatalytic experiments with 0.59 ppm NO$_x$ (0.35 ppm NO and 0.24 ppm NO$_2$) we monitored the photocatalytic conversion of NO and NO$_2$ on N-TiO$_2$ sample S2, under irradiation at $\lambda > 450$ nm for 60 min. We observed that, NO decreased by 82% (Fig. 6a) while the amount of NO$_2$ increased (not shown) by 25%. In accordance with this the measured overall removal of NO$_x$ was 65%, a value which is lower than that observed by Spadavecchia et al. [15] who also carried out measurement in the batch mode. It is worth noting, however, that in contrast to our experimental conditions, the N-TiO$_2$ photocatalyst was irradiated with light of wavelength in the range 380–600 nm and, in this case, the effect of the UV component cannot be neglected.

Accumulation of NO$_2$ from NO photooxidation, in the case of TiO$_2$, is a peculiar behaviour observed by different authors [48–50]. The common, and sensible explanation is that when NO$_2$ is formed by NO photooxidation, it can in part accumulate in the gas phase due to a limited availability of active sites [49].

For practical purposes of photocatalysis, however, the limited adsorption capability of TiO$_2$ requires its combination with a photochemically inert adsorbent that appears to play a key role in determining the overall photocatalytic efficiency. Indeed, several research works report on the low storage capability of TiO$_2$ toward NO$_x$ and on the beneficial effects of using composite materials consisting of TiO$_2$ dispersed in materials with high adsorbing power such as, e.g., active carbon, zeolites and hydroxyapatite [43,51,52]. In this context, we examined the abatement of NO$_x$ on N-TiO$_2$ mechanically dispersed into CaCO$_3$ as a model in view of perspective application in photocatalytically active construction and architectural materials [53].

Fig. 7 shows a comparison of UV–visible reflectance spectra of pure N-TiO$_2$ (S2) and its mixtures with CaCO$_3$. The spectrum of the latter is also displayed. Absorption in the visible region remain quite good even for the "diluted" photocatalyst and the activity of these mixtures for abatement of NO are excellent for the case of N-TiO$_2$ (10%) at $\lambda > 420$ nm (Fig. 8a). We underline that in addition to the removal of NO, the use of the composite catalyst bring about a consistent removal of NO$_2$ (Fig. 8b), at variance with the case of pure N-TiO$_2$ discussed above. Abatement of NO$_2$ still does not appear to be ideal since it is about 50% of the initial amount, but it represents a considerable improvement. Interestingly, inspection
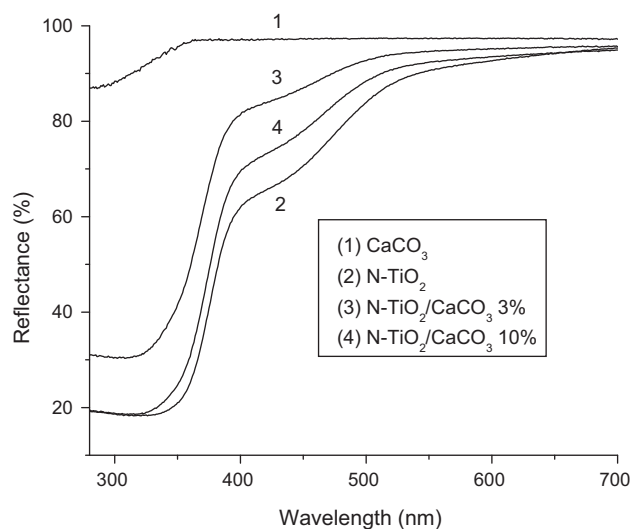

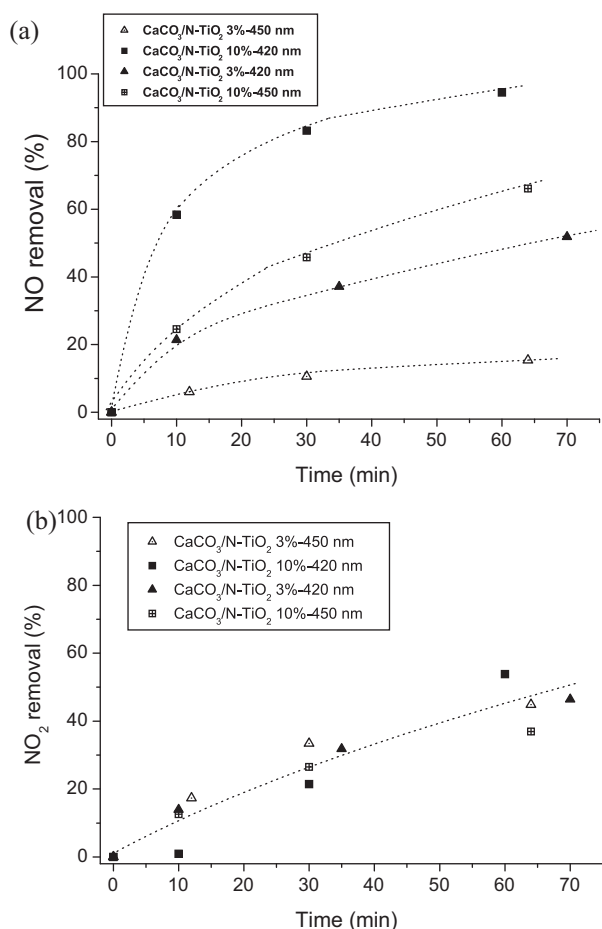**Fig. 7.** Diffuse reflectance UV–visible spectra (DRS) of pure N-TiO$_2$ (sample S2) or mechanically mixed with CaCO$_3$.

Fig. 8. Removal of NO (a) and NO_2 (b) as a function of time on N-TiO$_2$ (sample S2) mechanically mixed with CaCO$_3$. Irradiations in different wavelength regions selected with cut-off filters under batch conditions.

Fig. 9. Visible light ($\lambda > 400$ nm) photocatalytic degradation of 2-propanol ($\blacklozenge$) and variation of acetone ($\blacksquare$) and CO$_2$ ($\blacktriangle$) concentration in the presence of the samples (a) S0 and (b) S2. The initial concentration of the substrate injected inside the reactor was 15 μM.

of Fig. 8b reveals that removal is seemingly independent of light wavelength and of the amount of N-TiO$_2$ in the mixture which can be explained by prevailing adsorption effects of NO$_2$ on the photochemically inert CaCO$_3$ component. The next step in view of an enhancement in the overall NO$_x$ abatement is then a careful study on the most opportune absorbing matrix to be used in combination with the photocatalyst.

3.2.2. Photodegradation of 2-propanol

2-Propanol is often used as probe molecule for the evaluation of the photoactivity of TiO$_2$ at the gas/solid interphase, under UV and visible light irradiation [44,54,55]. Ihara et al. [55] prepared a non stoichiometric visible light active TiO$_2$ photocatalyst by plasma reduction treatment that showed an excellent activity toward benzoic acid and 2-propanol degradation. The authors attributed the vis-activity to oxygen vacancy state between the valence and the conduction band as visible light can excite electrons from the valence band to the oxygen vacancy state.

The photocatalytic activity of the samples studied in this paper both under UV and visible irradiation of the samples was determined employing the photodegradation of 2-propanol. The main intermediate product was acetone that was further oxidised to CO$_2$.

Photo-oxidation of 2-propanol under UV irradiation in the presence of samples S0 and S2 occurred with the same mechanism and with essentially the same rate (data not reported for the sake of brevity). A fraction of the 2-propanol was adsorbed on the catalyst surface and reacted as adsorbed species. It was then oxidised to CO$_2$ and partly to acetone which accumulates in the gas phase. The
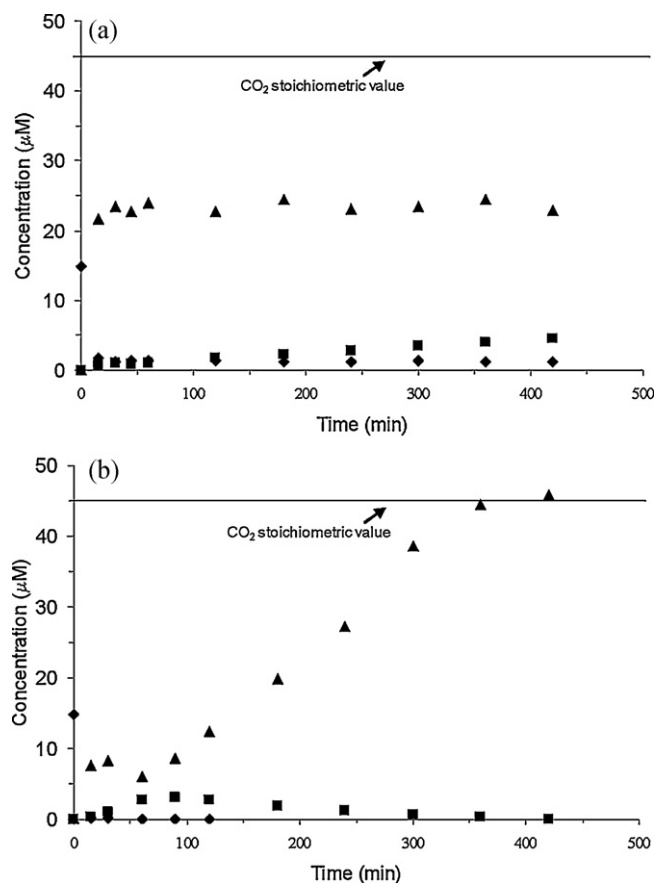
concentration of acetone reached a maximum value then decreased and disappeared from the gaseous phase after 2 h. The concentration of carbon dioxide reached the stoichiometric value after 3–4 h irradiation. Repeated photocatalytic runs did not show significant variations indicating that no catalyst deactivation occurred.

Fig. 9a shows the disappearance of 2-propanol under visible light irradiation ($\lambda > 400$ nm) versus irradiation time in the presence of the sample S0. After about 7 h irradiation small amounts of 2-propanol and acetone were present in the reactor and the concentration of CO$_2$ measured in the gaseous phase was half the stoichiometric value. This represents the maximum photo-activity that can be observed for S0 under irradiation in the full visible light region. No mass balance was obtained and this indicates that some species, including the reacting 2-propanol, probably remain adsorbed onto the surface. On the other hand, the photocatalyst become inactive when irradiation is carried on at wavelengths above 420 nm, as observed in the case of NO$_x$ (*vide supra*).

In Fig. 9b are reported analogous results for the photodegradation of 2-propanol on sample S2. Under these conditions, the activity of this photocatalyst is clearly higher than the undoped catalyst S0. After about 7 h of irradiation acetone disappeared and simultaneously the concentration of CO$_2$ reached the value corresponding to the total mineralization of 2-propanol.

For application purposes, as discussed above for the case of NO$_x$ conversion, some tests of 2-propanol photodegradation on N-TiO$_2$ (sample S2) in a CaCO$_3$ matrix (10% TiO$_2$) were carried out. Fig. 10 shows that while visible light irradiation caused the disappearance of 2-propanol in about 2 h, acetone is accumulated and is still present after 8 h continuous irradiation. The CO$_2$
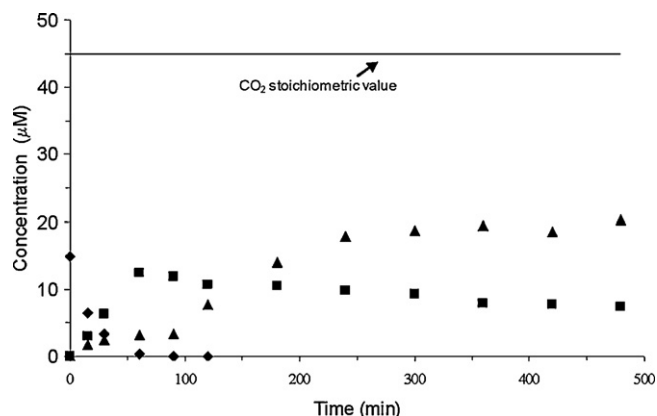
Fig. 10. Photocatalytic degradation of 2-propanol (♦) and variation of acetone (■) and CO_2 (▲) concentration in the presence of the sample S2(10)%-$CaCO_3$. The initial concentration of the substrate injected inside the reactor was 15 μM.

concentration reached a maximum of 15 μM, i.e. approximately one third of the stoichiometric amount. Photodegradation is still appreciable although comparison with the results discussed above for the pure sample S2 shows the expected loss of photoactivity.

4. Conclusions

N–doped samples were prepared by sol–gel methods starting from $TiOSO_4$ as the precursor and, for comparison, one sample was obtained by hydrolysis of titanium iso-propoxide. All the powders are constituted by pure anatase TiO_2 and present similar morphological characteristics. In particular, the doped samples showed absorption in the visible region but nitrogen did not modify the band- gap value. XPS analysis revealed a signal at 400 eV attributed to nitrogen in the form of Ti—N—O and EPR measurements confirmed the presence of molecular NO trapped with cavities/defect, likely interacting oxygen vacancies.

In general, the nitrogen-doped materials feature a good visible light photoactivity. The sample obtained by hydrolysis of $TiOSO_4$ with ammonia up to pH 7 has proved to be efficient for visible mineralization of 2-propanol and for the NO_x abatement. In the latter case, the measured photonic yields are 0.95 at 360 nm and 0.59 at 436 nm.

In view of perspective application in photocatalytically active construction and architectural materials, abatement of both NO_x and 2-propanol was also investigated using mechanical dispersions of up to 10% N-TiO_2 in photochemically inert $CaCO_3$. These composite materials maintain a quite good photocatalytic activity.

Acknowledgement

References

[1] T.L. Thomson, J.T. Yates, Chem. Rev. 106 (2006) 4428.
[2] X. Chen, S.S. Mao, Chem.Rev. 107 (2007) 2891.
[3] A. Fujishima, X. Zhang, D.A. Tryk, Surf. Sci. Rep. 63 (2008) 515.
[4] A.V. Emeline, V.N. Kuznetsov, V.K. Rybchuk, N. Serpone, Int. J. Photoenergy 2008 (2008) 19, Article ID 258394, and references therein.
[5] P.F. Ji, M. Takeuchi, T.M. Cuong, J.L. Zhang, M. Matsuoka, M. Anpo, Res. Chem. Intermed. 36 (2010) 327.
[6] S. Livraghi, M.C. Paganini, M. Chiesa, E. Giamello, Res. Chem. Int. 33 (2007) 739.
[7] R. Asahi, T. Morikawa, T. Ohwaki, K. Aoki, Y. Taga, Science 293 (2001) 269.
[8] T. Hirai, I. Tari, J. Yamaura, Bull. Chem. Soc. Jpn. 51 (1978) 3057.
[9] S. Livraghi, M.C. Paganini, E. Giamello, A. Selloni, C.D. Valentin, G. Pacchioni, J. Am. Chem. Soc. 18 (2006) 15666.
[10] C.D. Valentin, G. Pacchioni, A. Selloni, S. Livraghi, E. Giamello, J. Phys. Chem. B 109 (2005) 11414.
[11] S. Livraghi, A.M. Czoska, M.C. Paganini, E. Giamello, J. Solid State Chem. 182 (2009) 160.
[12] N. Serpone, J. Phys. Chem. B 110 (2006) 24287.
[13] A.V. Emeline, N.V. Sheremetyeva, N.V. Khomchenko, V.K. Rybchuk, N. Serpone, J. Phys. Chem. C 111 (2007) 11456.
[14] Y. Wang, C. Feng, M. Zhang, J. Yang, J. Zhang, Appl. Catal. B: Environ. 100 (2010) 84, and refs. therein.
[15] F. Spadavecchia, G. Cappelletti, S. Ardizzone, C.L. Bianchi, S. Cappelli, C. Oliva, P. Scardi, M. Leoni, P. Fermo, Appl. Catal. B: Environ. 96 (2010) 314.
[16] L. Samiolo, M. Valigi, D. Gazzoli, R. Amadelli, Electrochim. Acta 55 (2010) 7788.
[17] H.M. Yates, M.G. Nolan, D.W. Sheel, M.E. Pemble, J. Photochem. Photobiol. A: Chem. 179 (2006) 213.
[18] P. Pichat, in: M.A. Tarr (Ed.), Chemical Degradation Methods for Wastes and Pollutants: Environmental and Industrial Applications, Marcel Dekker, Inc., New York/Basel, 2003, pp. 77–119.
[19] J. Disdier, P. Pichat, D. Mas, J. Air Waste Manage. Assoc. 55 (2005) 88.
[20] A.G. Agrios, P. Pichat, J. Appl. Electrochem. 35 (2005) 655.
[21] J. Mo, Y. Zhang, Q. Xu, J.J. Lamson, R. Zhao, Atmos. Environ. 43 (2009) 2229.
[22] Y. Paz, Appl. Catal. B: Environ. 99 (2010) 448.
[23] T. Sano, N. Negishi, K. Koike, K. Takeuchi, S. Matsuzawa, J. Mater. Chem. 14 (2004) 380.
[24] S. Yin, H. Yamaki, M. Komatsu, Q. Zhang, J. Wang, Q. Tang, F. Saito, T. Sato, J. Mater. Chem. 13 (2003) 2996.
[25] I. Nakamura, N. Negishi, S. Kutsuna, T. Ihara, S. Sugihara, K. Takeuchi, J. Mol. Catal. A: Chem. 161 (2000) 205.
[26] T. Ihara, M. Miyoshi, Y. Iriyama, O. Matsumoto, S. Sugihara, Appl. Catal. B: Environ. 42 (2003) 403.
[27] Y. Yokosuka, K. Oki, H. Nishikiori, Y. Tatsumi, N. Tanaka, T. Fujii, Res. Chem. Intermed. 35 (2009) 43.
[28] W.K. Jo, J-T. Kim, Environ. Eng. Res. 13 (2008) 171.
[29] H. Irie, Y. Watanabe, K. Hashimoto, J. Phys. Chem. B 107 (2003) 5483.
[30] M. Miyauchi, A. Ikezawa, H. Tobimatsu, H. Irie, K. Hashimoto, Phys. Chem. Chem. Phys. 6 (2004) 865.
[31] M. Bellardita, M. Addamo, A. Di Paola, L. Palmisano, A.M. Venezia, Phys. Chem. Chem. Phys. 11 (2009) 4084.
[32] M. Bestetti, D. Sacco, M.F. Brunella, S. Franz, R. Amadelli, L. Samiolo, Mater. Chem. Phys. 124 (2010) 1225.
[33] C. Di Valentin, E. Finazzi, G. Pacchioni, A. Selloni, S. Livraghi, M.C. Paganini, E. Giamello, Chem. Phys. 339 (2007) 44.
[34] F. Peng, L. Cai, H. Yu, H. Wang, J. Yang, J. Solid State Chem. 181 (2008) 130.
[35] M. Mrowetz, W. Balcerski, A.J. Colussi, M.R. Hoffmann, J. Phys. Chem. B 108 (2004) 17269.
[36] A. Orlov, M.S. Tikhov, R.M. Lambert, C.R. Chimie 9 (2006) 794.
[37] S. Livraghi, A. Votta, M.C. Paganini, E. Giamello, Chem. Commun. (2005) 498.
[38] P. Mei, M. Henderson, A. Kassiba, A. Gibaud, J. Phys. Chem. Solids 71 (2010) 1.
[39] C. Feng, Y. Wang, Z. Jin, J. Zhang, S.Z. Wu, J. Zhang, New J. Chem. 32 (2008) 1038.
[40] X. Zhou, F. Peng, H. Wang, H. Yu, J. Yang, J. Solid State Chem. 184 (2011) 134.
[41] C.H. Ao, S.C. Lee, S.C. Zou, C.L. Mak, Appl. Catal. B: Environ. 49 (2004) 187.
[42] W. Belcerski, S.Y. Ryu, M.R. Hoffman, J. Phys. Chem. C 111 (2007) 15357.
[43] A.G. Agrios, P. Pichat, J. Photochem. Photobiol. A: Chem. 180 (2006) 130.
[44] Y. Sun, T. Egawa, L. Zhang, X. Yao, J. Mater. Sci. Lett. 22 (2003) 799.
[45] C. Feng, Z. Jin, J. Zhang, Z. Wu, Z. Zhang, Photochem. Photobiol. 86 (2010) 1222.
[46] D. Li, H. Haneda, N.K. Labhsetwar, S. Hishita, N. Ohashi, Chem. Phys. Lett. 401 (2005) 579.
[47] Y. Lei, D. Zhang, G.W. Meng, G.H. Li, Y.Y. Zhang, C.H. Liang, W. Chen, S.X. Wang, Appl. Phys. Lett. 78 (2001) 1125.
[48] T. Ibusuki, K. Takeuchi, J. Mol. Catal. 88 (1994) 93.
[49] C.H. Ao, S.C. Lee, J.C. Yu, J. Photochem. Photobiol. A: Chem. 156 (2003) 171.
[50] R. Amadelli, L. Samiolo, Concrete containing TiO_2 – an overview of photocatalytic NO_x abatement, in: P. Baglioni, L. Cassar (Eds.), Photocatalysis, Environment and Construction Materials, RILEM Publications S.A.R.L, Bagneux, France, 2007, pp. 155–162.
[51] K. Hashimoto, K. Wasada, M. Osaki, E. Shono, K. Adachi, N. Toukai, H. Kominami, Y. Kera, Appl. Catal. B: Environ. 30 (2001) 429.
[52] H. Yamashita, Y. Ichihashi, M. Anpo, M. Hashimoto, C. Louis, M. Che, J. Phys. Chem. 100 (1996) 16041.
[53] M. Borsa, R. Amadelli, L. Samiolo, L. Palmisano, M. Bellardita, ITMI20082158 (2010), also published as FR2939327 (2010).
[54] C. Chen, H. Bai, S. Chang, C. Chang, W.R. Den, J. Nanopart. Res. 9 (2007) 365.
[55] T. Ihara, M. Miyoshi, M. Ando, S. Sugihara, Y. Iriyama, J. Mater. Sci. 36 (2001) 4201.